Seismic Retrofitting of RC Piers using Continuous Fiber Sheet with Large Fracturing Strain

Hadiyono Jaqin*, Hiroshi Nakai**, Tamon Ueda***, Yasuhiko Sato***, Jianguo Dai***

* M. of Eng., Division of Structural and Geotechnical Engineering, Hokkaido University, Kita-ku, Sapporo 060-8628
** M. of Eng., Department of Civil Engineering Design, Mitsui-Sumitomo Construction Co. Ltd., Shinjuku-ku, Tokyo 162-5788
*** D. of Eng., Division of Structural and Geotechnical Engineering, Hokkaido University, Kita-ku, Sapporo 060-8628

This paper presents the experimental findings of cyclic loading test of ten half scale model of reinforced concrete bridge pier which were retrofitted by external wrapping using continuous fiber sheet with large fracturing strain, such as Aramid, PEN (Polyethylene Naphthalate), and PET (Polyethylene Terephthalate / Polyester) materials. These specimens were tested under static axial (1MPa) and reversed horizontal loading to represent earthquake excitation. The key mechanical properties of these materials are low tensile modulus of elasticity and large fracturing strain. The objective of this experiment is to get the optimum solution to achieve 10 δ_y as the ultimate deformation. The experimental results on the hysteretic response of test piers, ductility analysis, energy dissipation, and shear deformation on the plastic hinge are presented. The existing formulae for ductility prediction of members with carbon and aramid sheet are not applicable to members with PET sheet.
Key Words: cyclic loading, external wrapping, large fracturing strain, ultimate deformation

1. Introduction

In the year of 2003, Sanriku Minami earthquake struck Japan and caused some damages in many Japan Railways (JR) bridge piers. Recently, there is an effort on retrofitting these structures. The main issue is how to retrofit these structures economically in terms of cost savings and retain the mechanical performances of these structures according to Seismic Design Standard for Railway Structures [1]. One of the solutions is to retrofit these structures by external wrapping using new type of continuous fiber materials.

When designed according to current seismic design philosophy, reinforced concrete (RC) bridge piers are expected to have inelastic response. For economical reasons, some inelastic deformations are allowed and reduced base shear forces are used. The ability of RC bridge piers to withstand severe earthquakes depends mainly on the formation of plastic hinges near the pier footing interface where input energy can be dissipated. The energy dissipation capacity of RC piers during earthquake excitations can be increased and high ductility values ensured by confining the plastic hinge regions.

Deformability of reinforced concrete members is as important as strength especially for seismic performances of structures. Steel is still an excellent material to achieve good deformability, since fracturing strain of steel is very high so that steel fracture does not control the deformability practically. Continuous fibers have been applied widely as concrete reinforcement during the last decade. The most typical application is for seismic retrofitting in which continuous fiber reinforcement is used as externally bonded reinforcement or jacketing reinforcement. The major setback with continuous fiber reinforcement is its small fracturing strain, which often becomes a direct cause of the ultimate deformation.

The main feature of PEN (Polyethylene Naphthalate) and PET (Polyethylene Terephthalate / Polyester) fibers are its high fracturing strain and low tensile strength and stiffness in comparison with carbon, aramid, and glass fibers. The most common polyester for fiber purposes is polyethylene terephthalate or simply PET. This is also the polymer used for many soft drink bottles and it is becoming increasingly common to recycle them after being used by remelting the PET and extruding it as fiber. This saves valuable petroleum raw materials, reduces energy consumption, and eliminates solid waste sent to landfills. In Japan, Polyacetal Fiber (PAF), PEN, and PET are used for geo-textile reinforcement for ground stability improvement.

Figure 1 shows the stress-strain of various materials. Previous studies show that large fracturing strain fiber, in this case polyacetal fiber, is less likely to fracture before a concrete column reaches its ultimate deformation [2-3]. This fact is different from that of carbon fiber. Lower strength and stiffness can be compensated by providing additional amount of material, however low fracturing strain cannot be compensated by additional amount of material.

The objective of the experiment is to investigate the shear strengthening and ductility enhancement effect from retrofitting of RC pier with large fracturing strain continuous fiber sheet materials and to get the optimum solution to

achieve 10 δ_y as the ultimate deformation, which is suggested in JR seismic design code for railway structures.

2. Outline of Experimental Work

2.1 Experimental Configuration and Loading Process

The experimental configuration and loading history are shown in Figures 2 and 3 respectively. A compressive vertical load of 160 kN (1 MPa) corresponding to the dead load of the superstructure was applied. Loading point displacement at the time when reinforcements nearest to the extreme fiber of the column's bottom section reached the yield strain was used as yield displacement (δ_y), to which the corresponding load is yield load (P_y). Cyclic loads were applied gradually by increasing the displacement amplitude. Only one cycle was applied for each increasing of displacement amplitude. The ultimate deformation was defined as the displacement amplitude after passing maximum flexural capacity until its drop back to P_y under either push or pull loading condition.

2.2 Details of Specimens

In total 10 specimens were prepared (see Table.1). Each specimen consisted of a column part cast integrally with a bottom part. The column part represented a pier column of a regular bridge while the bottom part represented the footing of the pier. All the columns had section area of 400 x 400mm. Specimens with shear span 1150 mm (SP-1 to SP-5 in Table 1) had 1500 column height and footing dimension of 1100 x 600 x 1050 mm. The left specimens (SP-6 to SP-10 in Table 1) with shear span 1500 mm had 1850mm column height and footing dimension of 1100 x 600 x 700 mm.

Longitudinal reinforcements in all specimens had diameter of D19 and were embedded into footing parts. The reinforcing ratio of longitudinal bars ranged from 0.78 % to 1.18 %.(see Fig.4). Tie reinforcements had diameter of D6 and space of 100mm (see Fig.4). The volumetric ratio of ties to the concrete core was 0.16 % for all specimens. Material properties of longitudinal bars, tie reinforcement and concrete can be found in Table 2. JSCE Design Recommendation was used for calculating shear and flexural capacity of all specimens. Under the designed longitudinal and transverse reinforcing ratio, two non-strengthened RC columns (see specimens SP-1 and SP-8 in Table 1) were expected to fail in shear. The specimen cross section was generally a half of that of a conventional rigid-frame railway viaduct pier. For the retrofitted specimens, the large fracturing strain materials were applied only in plastic hinge region, which is 40 cm from the bottom of the pier. High modulus aramid fiber was used as shear strengthening at the region beyond the plastic hinge for retrofitted specimens. The purpose it to make sure that the failure of the retrofitted specimen was concentrated at the plastic hinge region and to observe the effectiveness of using duplex fibers.

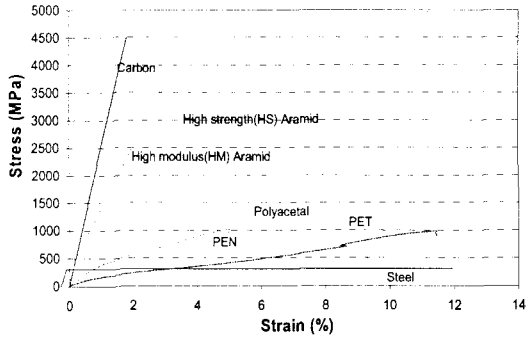

Fig. 1 Stress-strain curves of various materials

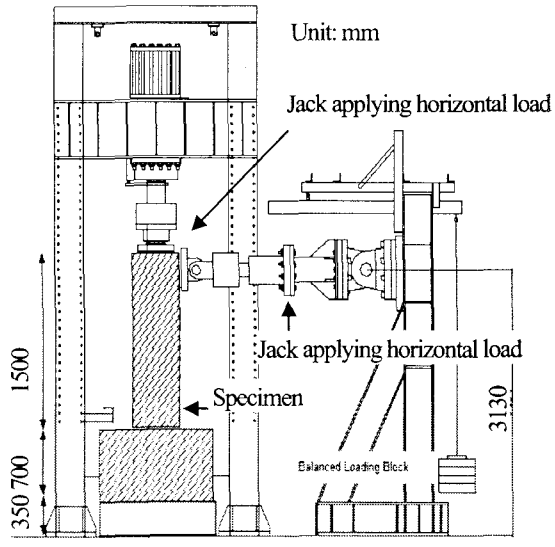

Fig. 2 Experimental device for first phase

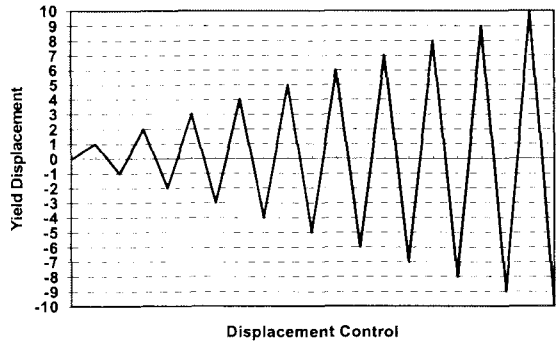

Fig. 3 Loading history

Section area of all column: 400×400mm

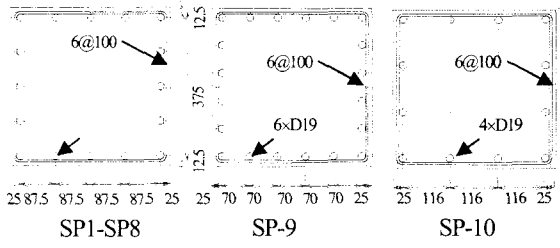

Fig. 4 Layout of longitudinal tie reinforcements

Table 1 Properties of specimens

Items	Unit	SP-1	SP-2	SP-3	SP-4	SP-5	SP-6	SP-7	SP-8	SP-9	SP-10
Dimension	mm	400*400									
Shear Span (a)	mm	1150					1500				
Axial Load	MPa	1.0									
Longitudinal bar		5@D19	5@D19	5@D19	5@D19	5@D19	5@D19	5@D19	5@D19	6@D19	4@D19
ρ_t		0.0098								0.0118	0.0078
Transverse ties		D6@100									
ρ_s		0.0016									
M_y	kNm	257								310	210
M_u	kNm	327								393	260
V_u	kN	284					218			262	173
V_c	kN	118								120	107
V_s	kN	73									
$(V_c+V_s)/V_u$		0.67					0.88			0.74	1.04
Sheet Reinforcement above Plastic Hinge Zone											
Material Type		-	High Modulus (HM) Aramid								-
ρ_f		-	0.00097	0.00097	0.00097	0.00048	0.00024	0.00024		0.00024	
V_f	kN	-	231	231	231	134	67	67		67	
$(V_c+V_s+V_f)/V_u$		0.67	1.48	1.48	1.48	1.14	1.18	1.18	0.88	0.99	1.04
Sheet Reinforcement on Plastic Hinge Zone											
Material Types		-	HSAramid*	PEN	PET	PET	PET	PET	-	PET	PET
ρ_f		-	0.00126	0.00382	0.00377	0.00187	0.00125	0.00063		0.00125	0.00063
V_f	kN	-	213	205	181.6	90.8	60.5	30.3		60.5	30.3
$(V_c+V_s+V_f)/V_u$		0.67	1.42	1.39	1.31	0.99	1.15	1.01	0.88	0.97	1.21
Ductility (Exp)		5.09	> 12	> 11	> 14	8.06	9.06	8.45	6.77	8.96	11.79

where: ρ_t: Tensile Reinforcement Ratio; ρ_s: Shear Reinforcement Ratio; M_y: Yielding Moment; M_u: Ultimate Moment; V_u: Ultimate Flexural Capacity; V_c: Shear Strength Capacity of Concrete; V_s: Shear Strength Capacity of Shear Reinforcement; ρ_f: Reinforcement Ratio; V_f: Shear Strength of Sheet; HSAramid: High Strength Aramid.

Table 2 Material properties

Items	E (GPa)	f_y (MPa)	f_t (MPa)	ε_{fu}
Longitudinal bars D19	176	394	-	-
Tie reinforcement D6	188	340	-	-
Aramid (high strength)	79.5	-	3246	0.041
PEN	22.6	-	1028	0.045
PET	6.7	-	923	0.138
Aramid (high modulus)	122	-	2670	0.022
Concrete	20	-	$\approx 30(f_c')$	-

where: E: Young Modulus; f_y: Yielding Strength; f_t: Maximum Tensile Strength; ε_{fu}: Fracturing Strain; f_c': concrete compressive strength.

2.3 Experimental Measurements

Strains in the continuous fiber and steel at various locations, deflections along the specimen length, and axial and lateral loads were monitored through the extensive use of instrumentation. The strain gages on continuous fiber sheet were attached on the four sides of piers. Also the employed were data logger, an A/D converter, and personal computers to control the input/output data. In order to observe the shear deformation of all columns at the plastic hinge region, many Linear Variable Displacement Transducer (LVDT) was set according to the configuration as shown in Figure 5.

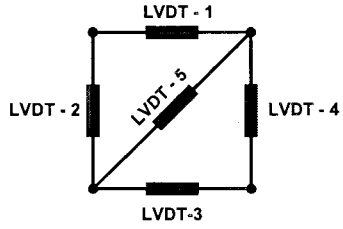

Fig. 5 LVDT Configuration for shear deformation measurement

3. Test Results and Discussions

The experimental activities were divided into 2 phases. The first phase aimed to get the most suitable material among high strength Aramid, PEN, and PET in order to achieve 10 δ_y as the ultimate deformation. SP-1 to SP-4 were tested for the first phase at Hokkaido University. The second phase aimed to know the optimum configuration using the most suitable material to achieve 10 δ_y as the ultimate deformation. In this case, SP-5 to SP-10 were tested for the second phase at Mitsui Sumitomo Research Center.

3. 1. First Phase Experimental Results

The load-displacement hysteretic loops for SP-3 are given in Figure 6. It can be seen that there is a stable load carrying capacity even the specimen was subjected to large deformation. It can be seen

that the behavior of this specimen during cyclic loading is very ductile. Until the last cycle of loading that is 11 δ_y, this specimen has not reached the ultimate deformation yet. The reversed cyclic loading was done until the specimen reached the maximum displacement capacity of horizontal hydraulic jack. The comparison of envelope curves for all specimens can be seen in Figure 7 and the condition for specimens after failure can be seen in Figure 6.

From Figure 7, it can be seen that there is a shear failure in SP-1,

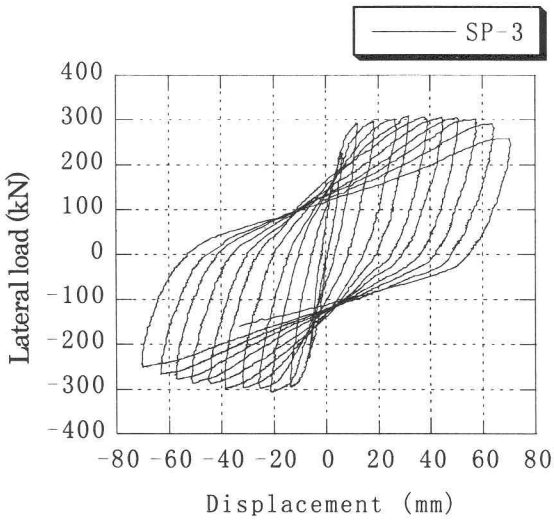

Fig. 6 Load displacement curve for SP-3 (PEN Fiber)

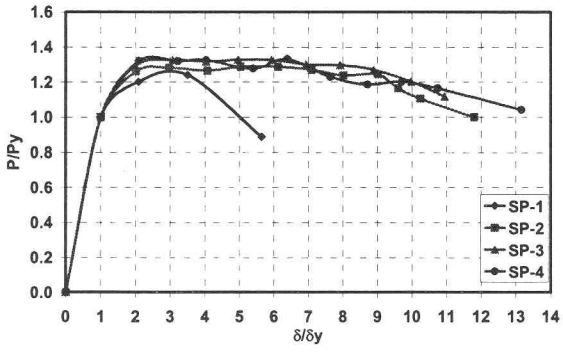

Fig. 7 Comparison of envelope curves

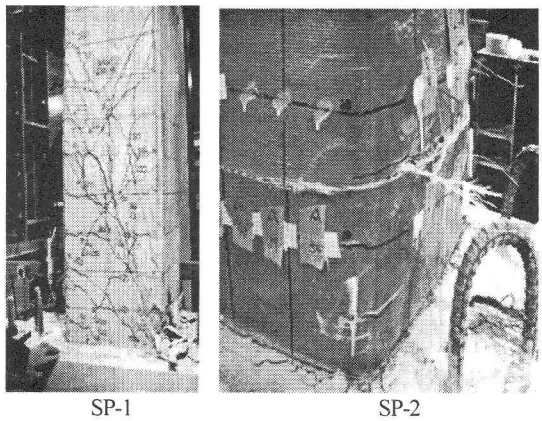

SP-1 SP-2

Fig. 8 Condition of specimen at ultimate condition

which is shown by sudden drop of shear resistance and formulation of shear diagonal cracking at the specimen. For SP-1, the failure mechanism is shear failure after yielding of reinforcement. However, for retrofitted specimens, the failure mechanism is yielding of the flexural reinforcing bar, reaching the ultimate flexural resistance, and then followed by buckling of longitudinal reinforcement at plastic hinge zone. For specimens retrofitted with PEN and PET, there is no fracture of the fiber itself until the end of test. On the contrary, there is a fracture of Aramid (high strength) fiber when the specimen reached 11 δ_y. This fracture is caused by the buckling at the plastic hinge zone as shown in Figure 8. The ultimate deformation for specimen retrofitted with high strength Aramid fiber is about 12. Because of the limitation of testing system, the ultimate deformation for specimen retrofitted with PEN and PET fiber cannot be obtained precisely.

From Figure 7, it can be seen that there is no significant increasing of load carrying capacity for the retrofitted specimens in comparison with the un-retrofitted specimen. Enwrapping above the plastic hinge zone is very effective to avoid shear failure and enwrapping along plastic hinge zone is very effective to restrain buckling of flexural reinforcement. The failure pattern of retrofitted specimens was moved from shear failure to flexural failure. This is because there are sheet reinforcements above and along the plastic hinge region. For the entire retrofitted specimens, it can be seen that their ductility is more than 10. The ductility here is defined as ratio of ultimate displacement to yield displacement. All of the retrofitted specimens show ductile phenomena, which means that they have stable shear resistance under large deformation. This is because of excellent confinement provides by continuous fibers (high strength Aramid, PET, and PEN) in the plastic hinge zone even when the deformation of the specimen becomes larger and larger.

Although the flexural reinforcements are buckled and there is loss of bond between concrete and reinforcement, the specimen can still have a good load carrying capacity. This is because there is no spalling of concrete so that the concrete even in crushing inside the pier still can contribute its strength at large deformation. Moreover, because of the nature of large fracturing strain fiber without yielding phenomena, the fiber itself still can give its strength as confinement while steel shear reinforcement was yielding when large deformation occurs. This mechanism makes load carrying capacity of retrofitted specimens remain stable. On the other hand, there will be some part of concrete spalling out when the continuous fiber was broken. The tensile force loss due to fiber fracture means not only the loss of confinement for the cover concrete but also the loss of shear force carrying capability as shear reinforcement, which reduces shear force carrying capacity of the pier.

In terms of unit price of continuous fiber material to get the same sheet strength, without considering the sheet processing cost, construction and transportation cost, the cost comparison shows aramid (high strength) : PEN : PET = 8 : 6 : 3. From this information, it can be concluded that continuous fiber with higher fracturing strain but lower Young's modulus is cheaper than continuous fiber with high Young's modulus and low fracturing strain. In this experimental

series, it can be concluded that PET fiber is the most efficient in terms of cost and seismic performance such as ductility and load carrying capacity. From this standpoint, second phase of experimental activity was conducted using PET fiber as reinforcing material in the plastic hinge zone.

3. 2. Second Phase Experimental Results

The behavior of the specimens was graphically presented in the form of relationships between the hysteretic pier shear force and the tip deflection.(see Fig. 9). Deflection was determined from readings of the upper LVDT located at the same level as the loading actuator. Yielding of the main and ties reinforcements, buckling of tensile reinforcement and fracturing of sheet enwrapping were marked on the hysteretic curves of the RC specimens. The starting point of buckling of flexural reinforcement was observed from sudden change of strain history pattern of flexural reinforcement. The failure mode for all specimens was also examined. All of specimens (SP-5 – SP-10) showed flexural failure followed by buckling of the tensile reinforcement. Axial-flexural failure in the hinge region could be seen for control specimen (SP-8), which is occurred when the pier develops its plastic flexural strength [4]. The pier is unable to develop significant flexural ductility due to inadequate confinement of the hinge region. Inadequate confinement of the concrete in the compression zone of the plastic hinge results in undesirable crushing of concrete. Load reversals further compound the deterioration of concrete in the plastic hinge region. Inadequate lateral support from transverse reinforcement allows the longitudinal bars to buckle. For the retrofitting specimens, ductile shear failure in the hinge region occurs when the pier develops its plastic flexural strength but ultimately fails in shear could be seen for this experimental series. Widening of the flexure-shear cracks in the hinge region under cyclic load after yielding of the longitudinal bars results in rapid deterioration of the shear capacity in the hinge region. In this series of experimental activities, SP-8 is used as control specimen for SP-6 to SP-10.

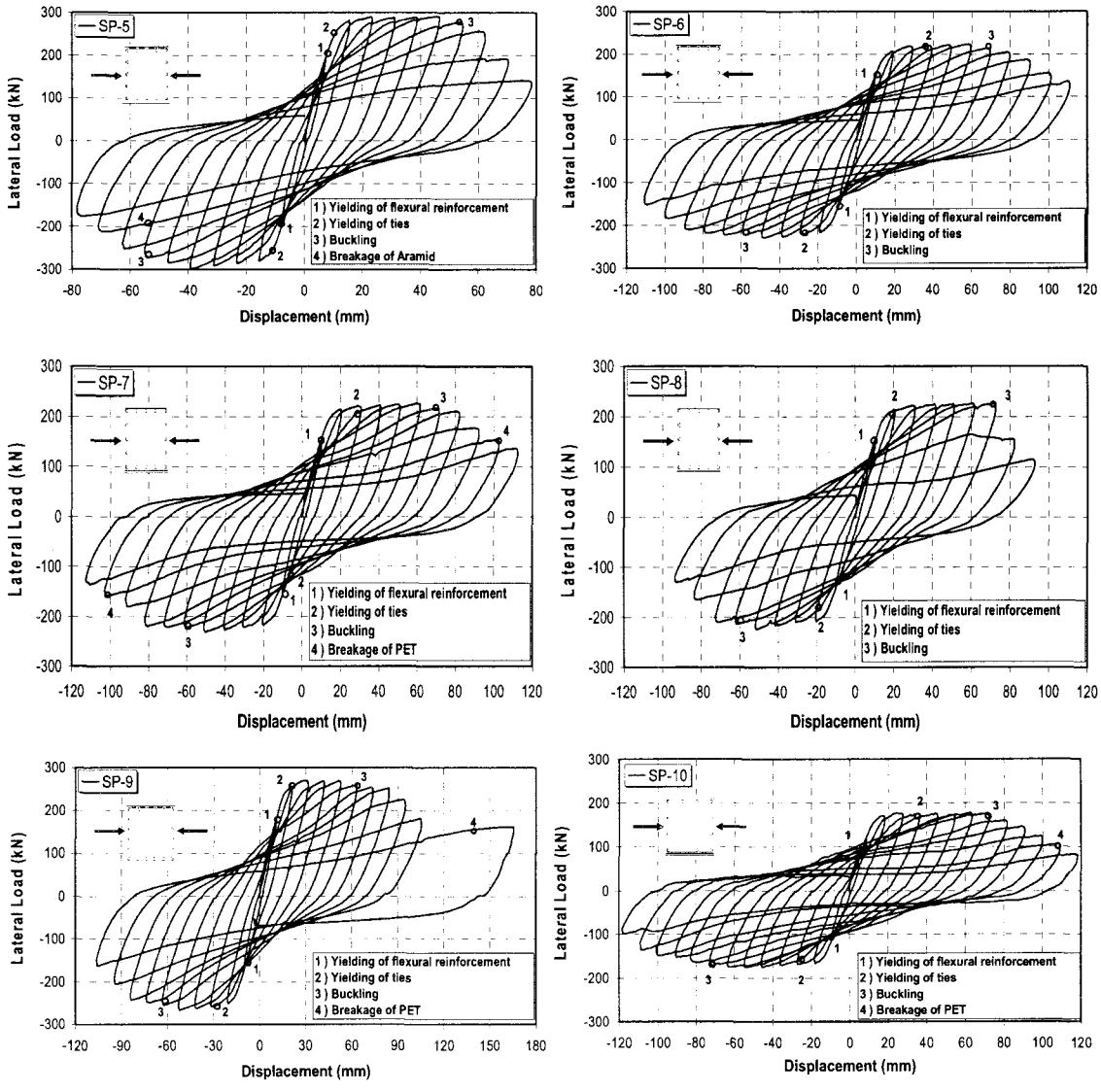

Fig. 9 Hysteric response of test piers

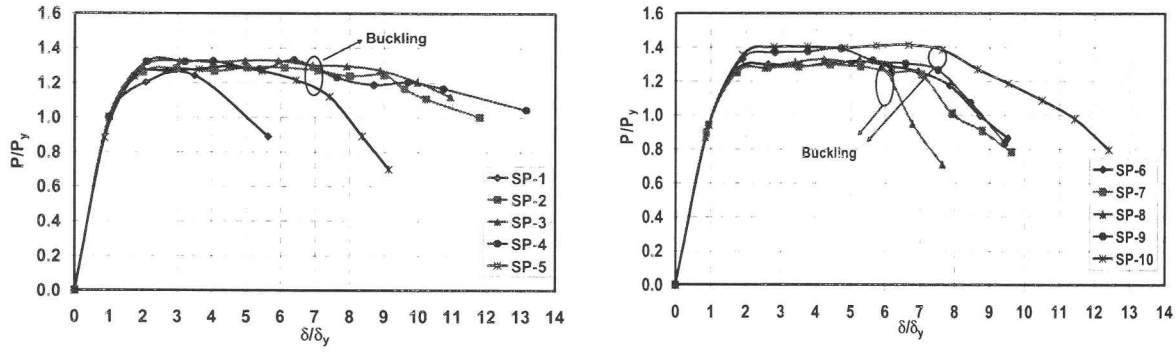

Fig. 10 Envelope curves for all specimens

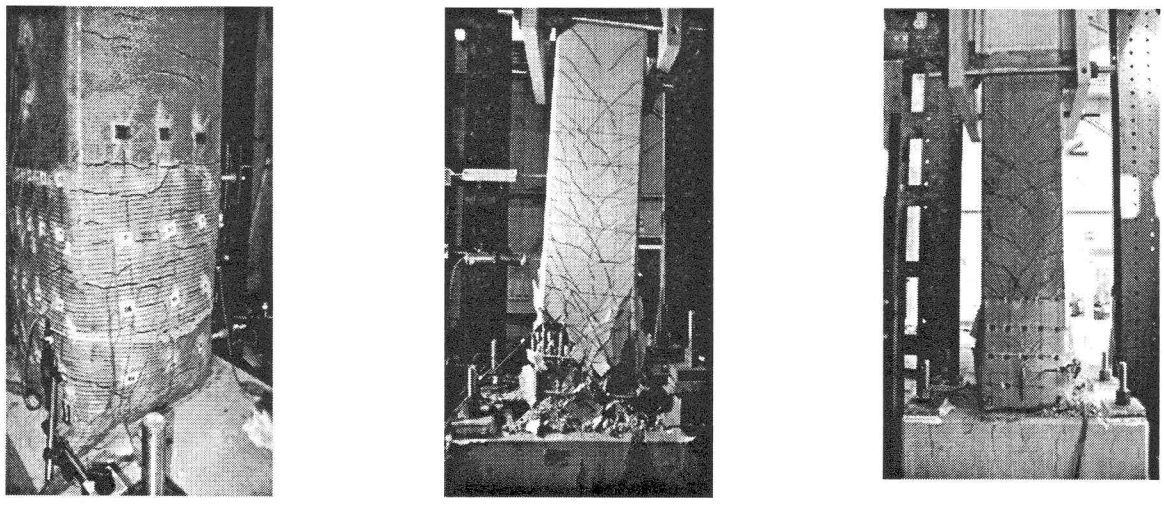

SP-6 SP-8 SP-10

Fig. 11 Condition of specimens at final stage of loading

The load-displacement hysteretic loops for SP-5 to SP-10 with the description when yielding of flexural reinforcement, yielding of ties, buckling of flexural reinforcement is clearly seen and breakages of sheet enwrapping are shown in Figure 9. The comparisons of the envelope curves for all specimens considering P-delta effect are shown in Figure 10. The condition of the specimens at final stage of loading cycle is shown in Figure 11

3. 2.1. Load Deformation Envelope Curves

From Figure 10, it can be seen that the enhancement of ductility for retrofitting using duplex continuous fiber sheet with large fracturing strain is more pronounce for un-retrofitted pier that has shear failure dominant (SP-1 to SP-5) than un-retrofitted pier that has flexural failure dominant (SP-6 to SP-10). The additional sheet reinforcement in SP-6 to SP-10 only enhances ductility after buckling causing the sudden drop of load carrying capacity. From Figure 11, it can be seen that most of the deterioration of RC pier happened at plastic hinge zone (the distance between 0 to 400 mm from the bottom of pier), so that the retrofitted action gives the optimum solution along this zone.

There are three parameters that are observed for the second phase of experiment. Those parameters are sheet reinforcement ratio, shear span, and tensile reinforcement ratio.

The hysteretic load-displacement curve for retrofitted RC pier reveals that, although the strength ratio was small, pinching was less pronounced. It was displayed for RC specimens that a fat hysteretic load-displacement curve was produced, allowing for high-energy dissipation during the cycles. Stable loops were recorded with no pinching which is usually associated with members having critical shear capacities. This is because the confinement effect of continuous fiber enhanced the concrete strength of ordinary RC piers.

For control specimen (SP-8), at high response ratios, concrete compressive strain in the plastic hinge regions exceeded the unconfined compression strain capacity, and concrete cover spalling was noticeable. It was not until the displacements were high that crushing began to penetrate inside the core concrete due to the large number of cycles.

(1) Effect of sheet reinforcement ratio on envelope curves

Specimens SP-6 to SP-8 are compared to investigate the effect of sheet reinforcement ratio on envelope curves of load displacement relationship as shown in Figure 12. The rate of decreasing of load carrying capacity after buckling of tensile reinforcement, which happened at the displacement level around 70 mm, is reduced with the additional of sheet enwrapping at the plastic hinge. The additional sheet reinforcement at plastic hinge gives confinement effect to the buckling of tensile reinforcement so that higher load carrying capacity could be achieved. Moreover, the sheet enwrapping could avoid concrete cover spalling so that the strength contribution from concrete will not decrease suddenly. These factors delay the reduction of load carrying capacity after buckling. Although the reinforcement ratio of SP-6 is twice as SP-7, the improvement of ultimate deformation is not significant. In this case, the additional sheet reinforcement only gives an effect after buckling of tensile reinforcement.

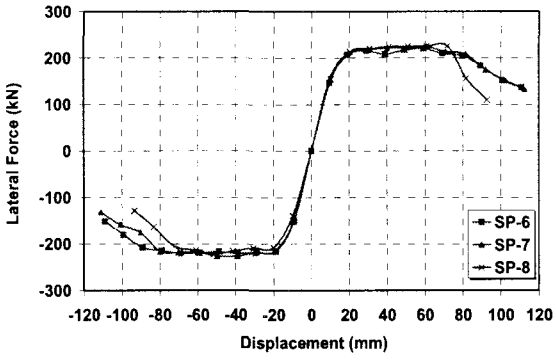

Fig. 12 Effect of sheet reinforcement ratio on envelope curves

(2) Effect of shear span on envelope curves

The effect of shear span could be observed at control specimen and retrofitted specimen. For control specimen (SP-1 and SP-8), the increasing of shear span makes the failure type move from shear to flexure. This is caused by the decreasing of flexural capacity of pier with the increasing of shear span so that the critical failure mechanism is moved from shear to flexure.

For retrofitted specimens, it can be observed that the higher the shear span the lower the load carrying capacity but the higher the value of ductility as it can be seen in Figure 13. This fact is in accordance with the calculated ultimate flexural capacity (V_u) in Table 1. Higher shear span causes higher shear-flexural strength ratio so that the flexural capacity derives the failure condition of the specimen. The tendency of flexural failure is more ductile than shear failure so that stable load carrying capacity for longer displacement ductility can be observed from flexural failure type.

(3) Effect of tensile reinforcement ratio on envelope curves

The effect of tensile reinforcement ratio could be seen in Figure 14. In this case it can be concluded that the higher the tensile reinforcement ratio, the higher the load carrying capacity. This fact is in accordance with the value of calculated ultimate flexural capacity (V_u) in Table 1.

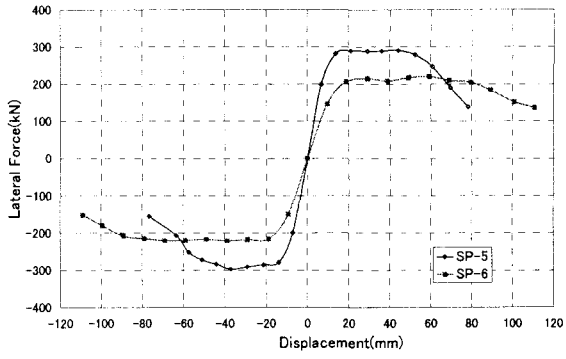

Fig. 13 Effect of shear span on envelope curves

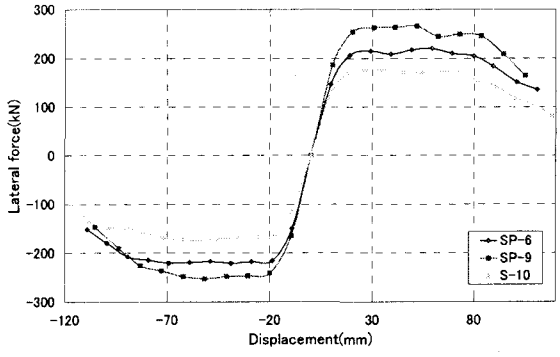

Fig. 14 Effect of tensile reinforcement ratio on envelope curves

3. 2 .2. Shear Deformation

As mentioned above, several LVDTs were used to measure the shear deformation of columns at the hinge zone (see Fig.15). The formation of LVDT and the sketch of shear deformation calculation can be expressed as shown in Figure 15.

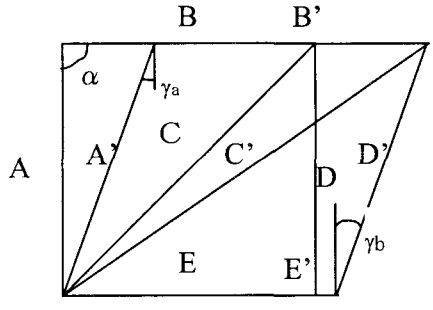

Fig. 15 Shear deformation sketch

From cosinus function, the following relationships can be obtained

$$C^2 = A^2 + B^2 - 2 \cdot A \cdot B \cdot \cos\alpha \quad (1)$$

$$C'^2 = A'^2 + B'^2 - 2 \cdot A' \cdot B' \cdot \cos(\alpha + \gamma_A) \quad (2)$$

$$(\alpha + \gamma_A) = \cos^{-1}\left(\frac{A'^2 + B'^2 - C'^2}{2 \cdot A' \cdot B'}\right) \quad (3)$$

$$\gamma_a = \cos^{-1}\left(\frac{A'^2 + B'^2 - C'^2}{2 \cdot A' \cdot B'}\right) - \alpha \quad (4)$$

With the same procedure, γ_B can be obtained as

$$\gamma_b = \cos^{-1}\left(\frac{D'^2 + E'^2 - C'^2}{2 \cdot D' \cdot E'}\right) - \alpha \quad (5)$$

$$\gamma_{average} = \frac{\gamma_a + \gamma_b}{2}, \quad (6)$$

The shear deformation of the rectangular section can be obtained as follows:

$$\delta_{shear} = \gamma_{Average} \cdot A \quad (7)$$

The cyclic shear deformation of SP-5 could be seen in Figure 16. From that figure, it can be seen that there is significant increasing of shear deformation especially after yielding of the shear reinforcement. The results of shear deformation versus lateral displacement of SP-5 to SP-10 can be seen in Figure 17. The percentage of shear deformation is getting higher after the yielding of shear reinforcement as it can be seen that the slope between lateral displacement and shear deformation decreases after the value of lateral displacement becomes higher than 30 mm for SP-6 to SP-10 and 20 mm for SP-5 at which the shear reinforcement yields. The influence of shear deformation is getting higher and higher as the increasing of lateral displacement.

(1) Effect of sheet reinforcement ratio on shear deformation

SP-6, SP-7 and SP-8 are compared to investigate the effect of sheet reinforcement ratio on shear deformation. It can be seen from Figure 16 that the higher the sheet reinforcement ratio, the lower the value of shear deformation at the same value of lateral displacement. This fact shows that the higher the value of sheet reinforcement ratio, the higher the effect of confinement at plastic hinge zone so that it will reduce the widening of flexure-shear cracks in the plastic hinge region under cyclic loading so that finally it will reduce the shear deformation.

(2) Effect of shear span on shear deformation

SP-5 is compared with SP-6 to investigate the effect of shear span on shear deformation. From Figure 16, it can be seen that shear span gives significant effect on the shear deformation development. The lower the shear span, the higher the value of shear deformation at the same value of lateral displacement. This is because the lower the shear span, the higher lateral force is needed to have the same value of flexural displacement. Under greater lateral force, there will be a greater shear deformation at the same value of lateral displacement.

(3) Effect of tensile reinforcement on shear deformation

SP-6, SP-9 and SP-10 are compared to investigate the effect of tensile reinforcement ratio on shear deformation. It can be seen in Figure 16 that there is no significant difference among those three curves until the displacement level of 60 mm. Because of crushing of concrete in plastic hinge region, the shear deformation beyond displacement level of 60 mm cannot be obtained for SP-10. In this case, SP-6 is compared with SP-9. From Figure 16, it can be seen that greater reinforcement ratio (SP-9) gives greater shear deformation at the same level of lateral displacement than SP-6. This fact is compatible with the fact that the higher the tensile reinforcement ratio, the greater the lateral (shear) forces to have the same flexural displacement. There should be a greater shear deformation under greater shear force. Therefore, the conclusion is the higher tension reinforcement ratio, the higher the ratio of shear deformation at the same value of lateral displacement.

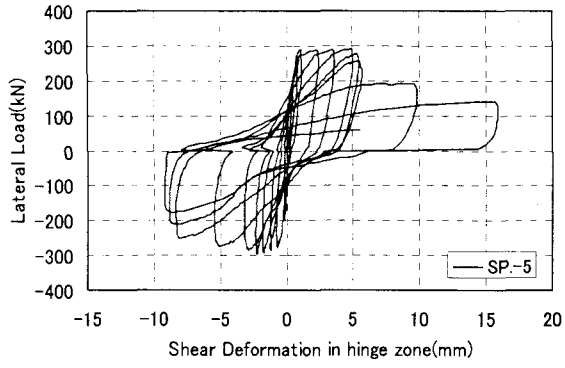

Fig. 16 Shear deformation history of SP-5

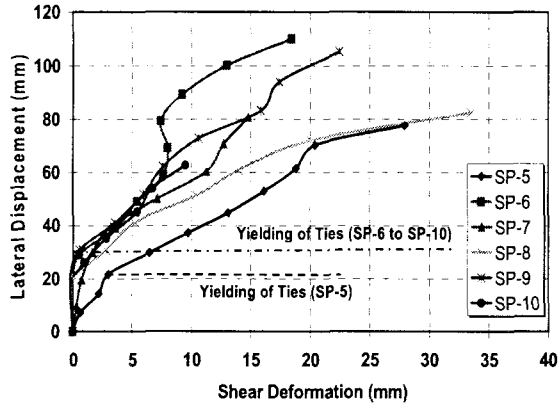

Fig. 17 Shear deformation versus lateral displacement

3. 2.3. Energy Dissipation

Energy dissipation is defined as area enclosing by load displacement curve for each cycle of loading. Figure 18 shows the value of energy dissipation for each displacement amplitude and Figure 19 shows the accumulated energy dissipation for each displacement amplitude. From Figure 18, it can be seen that the value of energy dissipation decrease after severe buckling of tensile reinforcement happened. The rate of decreasing of energy dissipation after severe buckling happened is lower for retrofitted specimen than for control specimen. Accumulated energy dissipation is calculated from the sum of energy

dissipation for each displacement amplitude. It can be seen from Figure 19 that as the displacement amplitude increases, the accumulated energy increases correspondingly.

(1) Effect of sheet reinforcement ratio on energy dissipation

SP-6, SP-7 and SP-8 are compared to investigate the effect of sheet reinforcement ratio on energy dissipation. From Figure 18, it can be seen that with the additional of sheet reinforcement, higher value of energy dissipation is obtained. From Figure 19, it can be seen that the maximum accumulated energy for control specimen (SP-8) is 127 kN.m. On the other hand, maximum accumulated energy dissipated for retrofitted specimens (SP-6 and SP-7) are around 190 kN.m. The accumulated energy dissipation for retrofitted specimen is 1.51 times that of control specimen, which shows the effectiveness of the sheet enwrapping for seismic retrofitting action. The increasing of sheet reinforcement ratio gives less significant effect to the accumulated energy dissipation as it can be seen that for SP-6 which is the reinforcement ratio is double than SP-7, the maximum accumulated energy dissipation for both retrofitted specimens almost the same.

(2) Effect of shear span on energy dissipation

SP-5 is compared with SP-6 to investigate the effect of shear span on energy dissipation. It can be seen from Figure 18 that longer shear span will give higher energy dissipation at the same level of displacement amplitude. Longer shear span makes the failure type is moved from shear (brittle) to flexure (ductile) so that better energy dissipation can be obtained. The maximum accumulated energy dissipation for SP-5 is 151.5 kN.m. while the maximum accumulated energy dissipation for SP6 is 193.8 kN.m.

(3).Effect of tensile reinforcement on energy dissipation

SP-6, SP-9 and SP-10 are compared to investigate the effect of tensile reinforcement ratio on energy dissipation. From Figure 18, it can be seen that the higher the value of tensile reinforcement ratio, the higher the value of energy dissipation at the same level of displacement amplitude. This phenomenon makes the development of accumulated energy dissipation is faster for higher tensile reinforcement ratio as it can be seen in Figure 19. The maximum value of accumulated energy dissipation for SP-6, SP-9 and SP-10 are almost the same.

3. 2.4. Ductility and Shear-Flexure Strength Ratio Relationship

From the experimental results, the relationship between ductility and shear-flexure strength ratio ($(V_c+V_s+V_f)/V_u$) of RC pier retrofitted by PET fiber can be seen in Figure 20. There is a good correlation between ductility and shear-flexure strength ratio which ductility increases as shear-flexure strength ratio increases. Figure 21 shows the comparison between ductility obtained from experimental results using PET fiber as retrofitting material and ductility calculated from present JSCE Formulation [5]. It can be

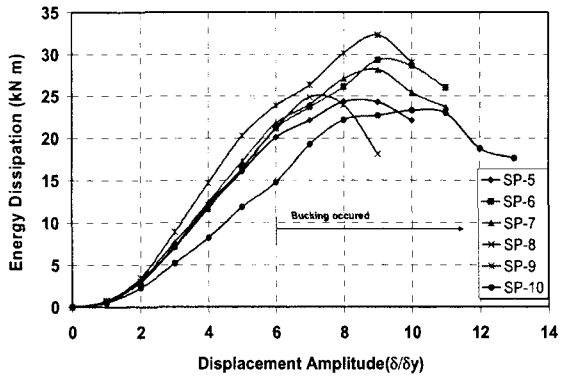

Fig. 18 Energy dissipation for each displacement amplitude

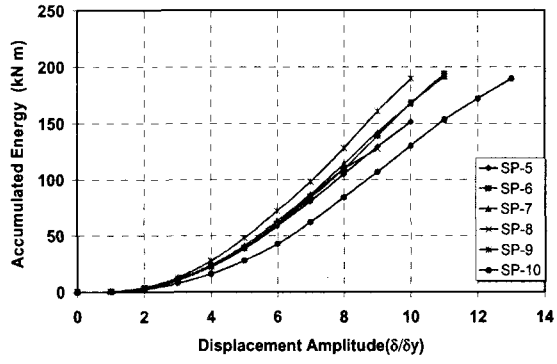

Fig. 19 Accumulated energy for each displacement amplitude

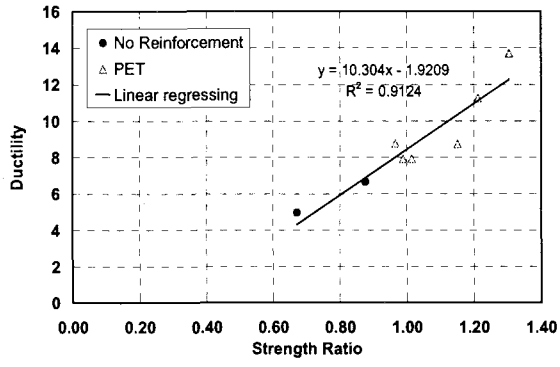

Fig. 20 Ductility and shear-flexure strength ratio relationship

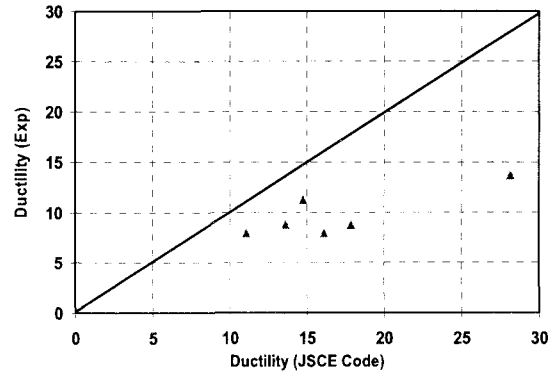

Fig. 21 Ductility comparison

seen that existing formula for ductility prediction, derived using the data for carbon and aramid fiber sheet, is not applicable to members with PET sheet and overestimates the experiment ductility. New design formula is needed.

4. Conclusions

1. Retrofitted by continuous fiber with large fracturing strain at plastic hinge region could increase the deformability of specimens, which can be greater than $10\,\delta_y$.
2. If the amount of sheet wrapped provides the equivalent strength, fiber with higher fracturing strain (PET) gives higher value of ductility of pier. In this case, high deformation of member without fracturing of continuous fiber is very important point to keep member load carrying capacity.
3. Retrofitting using large fracturing strain is more effective for RC pier that fails in shear rather than RC pier that fails in flexure.
4. Being retrofitted with large fracturing strain materials gives less significant effect on the load carrying capacity. On the other hand, enwrapping of RC pier with large fracturing strain materials gives more significant effect on the value of displacement ductility.
5. The retrofitted action at the plastic hinge region is effective after buckling of the specimen. It can be concluded that enwrapping with PET fiber is effective to prevent the deterioration of RC pier, especially at high value of deformation. At high value of deformation, PET fiber can prevent cover concrete from spalling-off due to buckling, so that it reduces the rate of strength deterioration after buckling.
6. The higher the sheet reinforcement ratio, the smaller the value of shear deformation.
7. Continuous fiber sheet with low elastic modulus but high fracturing strain can prevent the rapid increasing of shear deformation.
8. All of the retrofitted specimens show significant improvement of energy dissipation so that it is very effective for seismic retrofitting action.
9. The existing formula for ductility prediction derived using the data for carbon and aramid fiber sheet is not applicable to members with PET sheet.

Acknowledgements

The authors wish to express their appreciation for conducting this experiment to Mr. Tsutomu Kimura and Mr. Hideki Sato. The assistance of laboratory technicians of Mitsui Sumitomo Research Center is also acknowledged. Moreover, the authors express their gratitude to the Aramid Retrofitting System Association of Japan with the help for providing fiber sheets materials and to the experimental program.

References

1) Railway Technical Research Institute, *Seismic Design Code for Railway Structures*, Maruzen, 1999 (in Japanese).
2) Ueda T. and Sato Y., New Approach for Usage of Continuous Fiber as Non-Metallic Reinforcement of Concrete, *Structural Engineering International, International Association for Bridge and Structural Engineering (IABSE), Vol. 12, No. 2*, 2002,pp. 111 – 116.
3) Iihoshi C., Fukuyama H., Matsumoto Y., and Abe S., Strengthening Effect of Reinforced Concrete Elements with Polyacetal Fiber Sheets, *Proceeding of Fourth International Symposium on Fiber Reinforced Polymer Reinforcement for Reinforced concrete Structures, ACI Special Publication SP-188*, ACI, 1999, pp. 659 –669.
4) Sause R, Harries K.A., Walkup S.L., Pessiki S., and Ricles J.M., Flexural Behavior of Concrete Columns Retrofitted with Carbon Fiber-Reinforced Polymer Jackets. *ACI Structural Journal 101-S70*, September-October 2004, pp.708-716.
5) JSCE 292 Committee on Concrete Structures with Externally Bonded Continuous Fiber Reinforcing Materials, *Recommendation for Upgrading Concrete Structures with Use of Continuous Fiber Sheets*, Concrete Engineering Series 41, JSCE, 2001.

(Received on September 17, 2004)